Quantization of polariton states of rare-gas precipitates in metals with application to electron energy-loss spectra

I. Yu. Goliney and V. I. Sugakov
Institute for Nuclear Research, Academy of Sciences of Ukraine, prospekt Nauki 47, Kyiv 03680, Ukraine

Yu. V. Kryuchenko
Institute of Physics of Semiconductors, Academy of Sciences of Ukraine, prospekt Nauki 45, Kyiv 03680, Ukraine
(Received 26 April 2005; published 29 August 2005)

In the paper we present results of the calculations of the electron energy loss spectra of the rare-gas precipitates in metals. The theory of the inelastic scattering of fast electrons by the excitations localized on inclusions is developed. The excitations of the system are both quantized exciton-polariton levels of the precipitates and localized surface plasmons, which can strongly interact with each other. The angular dependence of the electron energy loss spectra is analyzed. It is shown that for the small angle scattering the structure of the electron energy loss spectrum is mainly due to the size quantization of excitonic levels. The levels closest to the surface polariton frequency are the strongest. At larger scattering angles the discrete structure of the electron energy loss spectrum is caused by the excitations with different orbital quantum numbers l and the separation of those levels is larger.

DOI: 10.1103/PhysRevB.72.075442 PACS number(s): 73.22.Lp, 79.20.Uv

I. INTRODUCTION

Rare-gas atoms introduced into metals by ion irradiation or as products of the radioactive decay tend to gather into bubbles due to low solubility. The behavior of the bubbles of noble gases in materials has been studied extensively because of problems associated with the development of fusion and fission reactors.[1]

Because of the high pressure of a gas in small size bubbles, rare-gas atoms in them form a crystalline phase that can exist up to the temperatures exceeding by much the melting temperature of the rare-gas crystals at normal conditions. For instance, crystallized Kr in Ni exists up to the temperature of 825–875 K, while at atmospheric pressure melting occurs at 115 K[2]. The phenomenon of the formation of the crystallites of the rare-gas atoms in metals has been a subject of intense studies for many years by a number of different methods, including x-ray diffraction,[2–13] neutron diffraction,[14] and the Mössbauer effect.[15] The rare-gas precipitates in metals form a truly unique system, where the crystal order exists at a very high temperature and very high pressure, the interatomic distances are small, and the symmetry of the crystallites is imposed by the host metal.

The recent studies[16,17] have attracted attention to the fact that such crystallites are, in fact, quantum dots for the excitons. As the oscillator strengths of the exciton transitions in the noble gas crystals are large, a strong mixing of the exciton and electromagnetic waves results, in fact, in the polariton nature of the quantized excitations of the precipitates. Additionally, the frequency of the atomic transitions of the rare-gas atoms are close to the frequencies of the plasmon excitations of the host metals (for example, aluminum). This leads to the strong mixing of the excitations in the precipitates and the plasmons, resulting in the strong enhancement of the spectral bands due to the excitations of the discrete quantized level of the excitations of the precipitates.[18]

The optical study of such systems, suggested in Refs. 16 and 17, is difficult for experiment due to the strong absorption. An alternative method is the study of the spectrum of the electron energy losses. In the present paper we develop a theory of the inelastic scattering of the incident high-energy electrons on the quantized excitations of the quantum dots in the form of the rare-gas precipitates. The technique of the electron energy loss spectra has been applied to the study of the rare-gas inclusions in metals and produced some interesting results.[19] In the present paper the theory of the inelastic scattering of electrons on a spherical inclusion with account for the spatial dispersion inside is extended to the case of nonzero scattering angles.

II. SPECTRUM OF EXCITATIONS OF A DIELECTRIC SPHERE IN A METAL TAKING INTO ACCOUNT THE EFFECTS OF THE SPATIAL DISPERSION

The spectrum of the electronic excitations of a dielectric sphere embedded in metal has been found and analyzed in Ref. 17 in the framework of the phenomenological approach as a solution of the system of Maxwell equations for the electric field and the model equations describing electrons inside and outside of the dielectric sphere. Here, only the starting equations and the expansions of the solutions necessary for the determination of the interaction of the external electron with the excitations are written down.

In the case when the wavelength of the electromagnetic field is much larger than the radius of the sphere, the quasistatic approximation can be used for the electric field. The electronic subsystems inside the sphere and outside of it is described within different model approaches. Outside the sphere, electrons are described classically by the Drude model of a free electron gas. Inside the dielectric sphere, where size quantization is important, a quantum mechanical model for the exciton polarization is used.

Outside of the sphere, in the metal, the free electron gas polarization in the Drude model and the electric field obey a following set of equations:

$$\varepsilon_{m0}\,\Delta\varphi - 4\pi\,\mathrm{div}\,\mathbf{P} = 0, \tag{1}$$

$$\ddot{\mathbf{P}} + \frac{\omega_p^2}{4\pi}\,\nabla\,\varphi = 0. \tag{2}$$

Solutions of this system of equations are sought in the form

$$\varphi = \sum_{l,m} a_{lm}(R/r)^{l+1} Y_{lm}(\theta,\varphi)e^{-i\omega t}, \tag{3}$$

$$\mathbf{P} = \sum_{l,m} b_{lm}\,\nabla\,[(R/r)^{l+1} Y_{lm}(\theta,\varphi)]e^{-i\omega t}; \tag{4}$$

$Y_{lm}(\theta,\varphi)$ are spherical harmonics. The substitution the ansatz solution into the set of equations gives a relationship between unknown coefficients a_{lm} and b_{lm}.

Inside the sphere, the dispersion effects and size quantization are described with the vector of exciton polarization that obeys the Maxwell equation in the electrostatic approximation,

$$\varepsilon_0\,\Delta\varphi - 4\pi\,\mathrm{div}\,\mathbf{P} = 0, \tag{5}$$

and an equation for the polarization derived from the Schrödinger equation in the case when excited levels are three times degenerate,

$$\ddot{\mathbf{P}} + \omega_0^2\mathbf{P} - \alpha\,\Delta\mathbf{P} + \beta\,\nabla\,\varphi = 0, \tag{6}$$

where $\alpha=\hbar\omega_0/M$ and M is the effective exciton mass. $\beta=\omega_{LT}\omega_0\varepsilon_0/2\pi$, where ω_{LT} is the transverse-longitudinal splitting, ω_0 is the frequency of the exciton band bottom for the material of the dielectric sphere, ε_0 is the low-frequency dielectric constant of the material of the sphere due to transitions other than the considered excitonic band.

The ansatz solution is

$$\varphi = \sum_{l,m} [c_{lm}^0 j_l(\kappa r) + c_{lm}^1 (R/r)^{l+1}] Y_{lm}(\theta,\varphi)e^{-i\omega t}, \tag{7}$$

$$\mathbf{P} = -\nabla\left[\sum_{l,m} (d_{lm}^0 j_l(\kappa r) + d_{lm}^1 (R/r)^{l+1}) Y_{lm}(\theta,\varphi)\right]e^{-i\omega t} + i\sum_{l,m} d_{lm}^2\,\mathrm{curl}[j_l(kr)\hat{\mathbf{L}}Y_{lm}(\theta,\varphi)], \tag{8}$$

where $j_l(x)$ are spherical Bessel functions, $\hat{\mathbf{L}}=-i[\mathbf{r}\times\nabla]$, $\alpha\kappa^2=\omega^2-\omega_0^2-4\pi\beta/\varepsilon_0$, and $\alpha k^2=\omega^2-\omega_0^2$.

The substitution of the ansatz solutions into Eqs. (6) gives relationships between the pairs of unknown coefficients c_{lm}^0 and d_{lm}^0, c_{lm}^1 and d_{lm}^1.

The sets of equations inside and outside the sphere should be completed with the boundary conditions at the interface. Besides the usual boundary conditions of the electrostatics,

$$\left(-\varepsilon_{m0}\frac{\partial\varphi}{\partial r} + 4\pi P_r\right)_{R+0} = \left(-\varepsilon_0\frac{\partial\varphi}{\partial r} + 4\pi P_r\right)_{R-0}, \tag{9}$$

$$\varphi(R+0) = \varphi(R-0). \tag{10}$$

An additional boundary equation for the exciton polarization is chosen in the form suggested by Pekar,[20]

$$P_r(R-0) = 0, \tag{11}$$

which assumes a specular reflection of excitons at the boundary of the dielectric sphere.

Boundary conditions allow us to find relationships between the all unknown coefficients. The additional boundary conditions determine the frequency spectrum of the electronic excitations by the equation with respect to ω:

$$\varepsilon_0 l + \varepsilon_{m0}(l+1) = l\frac{4\pi\beta}{\varepsilon_0(\omega^2-\omega_0^2)} \times \frac{S_l(k)\left(\varepsilon_0 R\frac{d}{dR}j_l(\kappa R) + \varepsilon_{m0}(l+1)j_l(\kappa R)\right)}{R\frac{d}{dR}[j_l(\kappa R)]\frac{d}{dR}[Rj_l(kR)] - l(l+1)j_l(\kappa R)j_l(kR)}, \tag{12}$$

where

$$S_l(x) = x\frac{dj_l(x)}{dx} - lj_l(x). \tag{13}$$

The roots of Eq. (12) include all different types of excitations that could be localized on the dielectric sphere with spatial dispersion in a metal matrix: excitonic and polaritonic excitations inside the sphere and localized surface plasmons; all types of excitations interact with each other.

III. QUANTIZATION OF THE EXCITATIONS. SCATTERING CROSS SECTION

In order to describe the interaction of the excitations found in the previous section with an external fast electron, one has to write down the Hamiltonian of the system in the second quantization approximation.

Following the established procedure, the quantization starts with the action

$$S = \int_{t_1}^{t_2} L\,dt. \tag{14}$$

The action has to be defined in such a way that the corresponding Lagrange equations,

$$\frac{d}{dt}\frac{\partial L}{\partial \dot{q}} - \frac{\partial L}{\partial q} = 0, \tag{15}$$

where q are the variables of the problem, which, in this particular case, are the electric field potential φ and the polarization $\mathbf{P}$, would produce the set of equations and boundary conditions describing the problem

$$S = \frac{1}{16\pi}\int_{t_1}^{t_2} dt\Bigg[\int_{r>R} d^3r\Bigg(\varepsilon_{m0}\nabla\varphi\ \nabla\varphi^* + 4\pi\varphi^*\,\mathrm{div}\mathbf{P} + 4\pi\varphi\,\mathrm{div}\,\mathbf{P}^* + \frac{(4\pi)^2}{\omega_p^2}\ddot{\mathbf{P}}^*\ddot{\mathbf{P}}\Bigg) + \int_{r<R} d^3r\Bigg(\varepsilon_0\ \nabla\varphi^*\ \varphi + 4\pi\varphi^*\,\mathrm{div}\mathbf{P} + 4\pi\varphi\,\mathrm{div}\,\mathbf{P}^* + \frac{4\pi}{\beta}\ddot{\mathbf{P}}^*\ddot{\mathbf{P}} - \frac{4\pi}{\beta}\mathbf{P}^*\mathbf{P} - \frac{4\pi\alpha}{\beta}(\mathrm{curl}\,\mathbf{P}^*\,\mathrm{curl}\mathbf{P} + \mathrm{div}\,\mathbf{P}^*\,\mathrm{div}\mathbf{P})\Bigg) + 4\pi R^2\int d\Omega(P_r^*\varphi + \varphi^* P_r)_{R+0}\Bigg]. \tag{16}$$

This action is completed by a requirement for the unknown functions φ and $\mathbf{P}$ to satisfy the boundary conditions

$$\varphi(R+0) = \varphi(R-0) \tag{17}$$

and

$$\mathbf{P}(R-0) = 0. \tag{18}$$

Taking variations of the fields one should demand that $\delta\varphi(R+0)=\delta\varphi(R-0)$ and $\delta\mathbf{P}(R-0)=0$.

Variations of the action of Eq. (16) with respect to the fields φ and $\mathbf{P}$ give the full system of equations and the boundary conditions

$$0 = \frac{\delta S}{\delta\varphi^*} = \begin{cases} -\varepsilon_{m0}\Delta\varphi + 4\pi\,\mathrm{div}\,\mathbf{P}, & r > R; \\ -\varepsilon_0\Delta\varphi + 4\pi\,\mathrm{div}\,\mathbf{P}, & r < R; \\ -\left(\varepsilon_{m0}\dfrac{\partial\varphi}{\partial r} + 4\pi P_r\right)_{R+0} + \varepsilon_0\dfrac{\partial\varphi}{\partial r}_{R-0}, & r = R. \end{cases} \tag{19}$$

$$0 = \frac{\delta S}{\delta\mathbf{P}^*} = \begin{cases} -(4\pi)^2/\omega_p^2\ddot{\mathbf{P}} - 4\pi\ \nabla\varphi, & r > R; \\ -4\pi/\beta\ddot{\mathbf{P}} - 4\pi\omega_0^2/\beta\,\Delta\mathbf{P} - 4\pi\ \nabla\varphi, & r < R. \end{cases} \tag{20}$$

The next step is to expand all unknown functions in a series of the eigenfunctions of the system determined in the previous section and obtain a classical Lagrange function depending on the expansion coefficients $a_{lm}(t)$ of Eq. (3) only,

$$\mathcal{L} = \frac{R}{16\pi}\sum_{l,m,i}(\ddot{a}^*_{lmi}\ddot{a}_{lmi} - \omega_{li}^2 a^*_{lmi}a_{lmi})B_{li}^2, \tag{21}$$

where B_{li}^2 is obtained by the integration

$$B_{li}^2 = \frac{\omega_p^2}{\omega_{li}^4}(l+1) + \frac{4\pi}{\beta}\left(\frac{\varepsilon_0 l + \varepsilon_{m0}(l+1)}{4\pi S(\kappa)}\right)^2 \times\Bigg(I_2(\kappa) + l(l+1)\frac{S_l^2(\kappa)}{l^2 S_l^2(k)}I_2(k) + \frac{4\pi\beta S_l(\kappa)}{\varepsilon_0(\omega_l i^2 - \omega_0^2)}\frac{\varepsilon_0 R\dfrac{d}{dR}j_l(\kappa R) + \varepsilon_{m0}(l+1)j_l(\kappa R)}{\varepsilon_0 l + \varepsilon_{m0}(l+1)}\Bigg), \tag{22}$$

$$I_2(x) = \frac{1}{2}\left[\left(x\frac{dj_l(x)}{dx}\right)^2 + xj_l(x)\frac{dj_l(x)}{dx} - [l(l+1) - x^2]j_l^2(x)\right]. \tag{23}$$

In the representation of the second quantization, one has to build a Hamiltonian on the basis of this classical Lagrange function,

$$\hat{H} = \frac{1}{2}\sum_{l,m,i}(\hat{A}^\dagger_{lmi}\hat{A}_{lmi} + \hat{A}_{lmi}\hat{A}^\dagger_{lmi})\hbar\omega_{li}, \tag{24}$$

where the creation and annihilation operators $\hat{A}^\dagger_{lmi}$ and $\hat{A}_{lmi}$, respectively, replace the classical amplitudes a_{lmi}.

The potential of the electric field can be represented by an operator,

$$\hat{\varphi} = \frac{1}{2}\sum_{l,m,i}[\hat{A}_{lmi}D_{li}g_{li}(r)Y_{lm}(\theta,\varphi) + \mathrm{c.c.}], \tag{25}$$

where

$$g_{li}(r) = \begin{cases} (R/r)^{l+1}, & r > R, \\ c^0_{lm}j_l(\kappa r) + c^1_{lm}(r/R)^l, & r < R, \end{cases} \tag{26}$$

$$D_{li}^2 = \frac{2\omega_{li}}{\hbar}B_{li}^2. \tag{27}$$

The relationship of the coefficients c^0_{lm} and c^1_{lm} with the classical amplitude a_{lm} was obtained in the previous section.

The Hamiltonian describing the interaction of an incident high-energy electron with the electric field of the electronic excitations localized on the spherical inclusion takes the form

$$\hat{H} = -\frac{\hbar^2\Delta}{2m} - e\hat{\varphi}, \tag{28}$$

where m is the electron mass and $\hat{\varphi}$ is given by Eq. (25).

Now, one can consider a process of the inelastic scattering of an incident electron from a state with the wave vector $\mathbf{K}$,

$$\psi_{in} = \frac{1}{\sqrt{V}}e^{i\mathbf{K}\mathbf{r}}, \tag{29}$$

to a state with the wave vector $\mathbf{K}'$,

$$\psi_f = \frac{1}{\sqrt{V}}e^{i\mathbf{K}'\mathbf{r}}. \tag{30}$$

Introducing a vector, $\mathbf{Q}=\mathbf{K}'-\mathbf{K}$, the matrix element of the transition becomes

$$-\frac{e}{2}D_{li}\langle \mathbf{K}'|g_{li}(r)|\mathbf{K}\rangle = -\frac{e}{2}(-i)^l\sqrt{\frac{2\pi}{V}}D_{li}\int_0^\infty r^2 j_l(Qr)g_{li}(r)dr. \quad (31)$$

The cross section of the inelastic scattering with the excitation of the lith mode in the sphere is

$$\frac{\sigma_{li}}{\Omega}=\frac{1}{4\pi}\left(\frac{em}{\hbar^2}\right)^2\sqrt{1-\frac{\hbar\omega_{li}}{\varepsilon_{\mathbf{K}}}}(2l+1)|D_{li}f_{li}(Q,R)|^2, \quad (32)$$

where

$$Q=K\left[2-\frac{\hbar\omega_{li}}{\varepsilon_{\mathbf{K}}}-2\cos\Theta\left(1-\frac{\hbar\omega_{li}}{\varepsilon_{\mathbf{K}}}\right)^{1/2}\right]^{1/2}, \quad (33)$$

Θ being the angle between $\mathbf{K}$ and $\mathbf{K}'$,

$$\varepsilon_{\mathbf{K}}=\frac{\hbar^2K^2}{2m}, \quad (34)$$

$$f_{li}=\frac{R}{Q^2}\left[(l+1)j_l(QR)+R\frac{\partial j_l(QR)}{\partial R}+c_{li}^0\frac{Q^2}{Q^2-\kappa^2}\left(R\frac{\partial j_l(\kappa R)}{\partial R}+j_l(QR)-R\frac{\partial j_l(QR)}{\partial R}j_l(\kappa R)\right)+c_{li}^1\left(lj_l(QR)-R\frac{\partial j_l(QR)}{\partial R}\right)\right]. \quad (35)$$

The spectrum of the excitations of a spherical inclusion is discrete. In order to obtain a continuous spectrum of the electron energy losses, each of the lines corresponding to the excitation of a discrete level has been approximated with a Lorentz curve,

$$f(\omega)=\frac{1}{\pi}\frac{\gamma}{(\omega-\omega_{l,i})^2+\gamma^2}, \quad (36)$$

where γ is a broadening factor, the same for all lines.

In order to decrease the dependence of the spectrum on the broadening factor and taking into account the fact that the radius of inclusions in metals has some scatter, the resulting spectrum was averaged over a certain radius range.

IV. NUMERICAL RESULTS AND DISCUSSION

One of the most prominent features of the system is the repulsion of the states of the atomic excitations inside the rare-gas inclusions and the localized plasmons. It is known that a free electron gas around a small void in a metal has its own excitations called localized plasmons. The spectrum of the localized plasmons in the case of a spherical void in a metal can be estimated by an equation,

$$\omega_l=\omega_p\sqrt{\frac{l+1}{2l+1}}, \quad (37)$$

where ω_l is the frequency of a localized plasmon and l is the orbital quantum number. With increasing l the levels converge to the frequency of a surface plasmon $\omega_p/\sqrt{2}$. It is important to note that the spectrum of the local plasmons does not depend on the radius of the voids, provided the voids are small enough, i.e. much smaller than the wavelength of light with the same frequency.

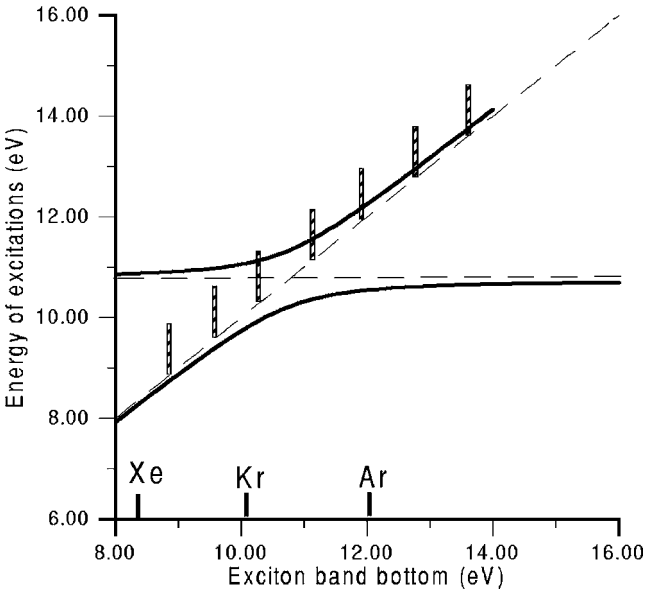

FIG. 1. The repulsion of states of the atomic excitations and localized plasmons as a function of the energy of exciton band bottom ω_0. The values of ω_0 for real noble gases are indicated.

In the case of rare-gas precipitates in the metal, the localized plasmons can interact with the atomic excitations of the gas atoms in the precipitate. This interaction leads to a strong mixing of the states and repulsion of their levels. This effect is demonstrated in Fig. 1 for the states with $l=1$. The effect is essential for the rare gases that have the frequency of the lowest transition below the plasmon frequency of the host metal. The magnitude of the frequency shift of the excitations in proportional to $\sqrt{\omega_{LT}\omega_p}$ and can reach up to 1 eV.

Another prominent feature of the spectrum of the excitations localized on the crystalline inclusions is the size quantization. The precipitates of the rare-gas atoms in metals can be rather small, i.e., of the order of several nanometers. Such small precipitates are examples of the quantum dots and the electronic or excitonic spectrum in them is quantized. The quantization is sensitive to the radii of the precipitates and is smeared down to a large extent in the spectra.

Figures 2–6 show the electron energy loss spectra of the spherical inclusions of the crystallites of different rare-gas atoms for the case of scattering forward, i.e., $\Theta=0$. For the calculations, the size of the precipitates was considered to vary in the range from 2.0 nm to 3.0 nm. All electron energy loss spectra were averaged in this range. The energy of the incident electron was chosen to be 20 keV. The parameters of the excitonic bands for the crystals were taken from the data obtained at normal pressure and low temperatures.[21] These values can undergo changes in the case of the rare gas in precipitates, yet these effects were not taken into account in the present paper. The broadening factor γ was taken to be 0.01 eV. In the case of the scattering forward, i.e., $\Theta=0$, the main contribution into the electron energy loss spectra comes

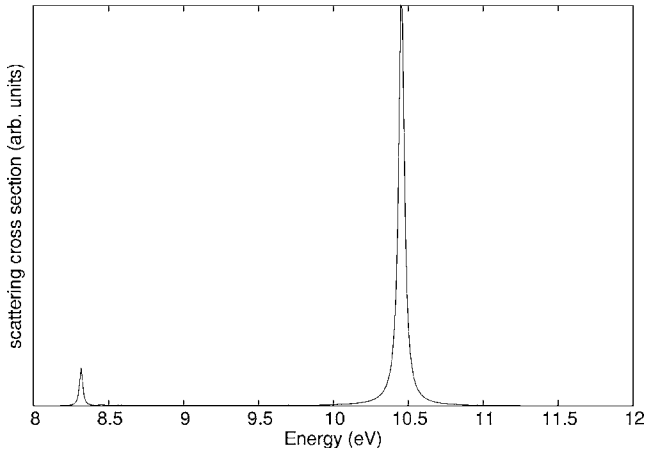

FIG. 2. EELS spectrum of Al with Xe precipitates for the scattering forward. Parameters of the Xe crystal in the precipitates are ω_0=8.36 eV, ω_{LT}=0.11 eV, ε_0=2.22, $M=2.2m_0$, where m_0 is the free electron mass.

from the dipole excitations with $l=1$. The same excitations are the most active in the optical spectra and contribute to the dielectric function of the metal with embedded precipitates.

The EEL spectrum of the Xe precipitates in Al in Fig. 2 does not show a strong shift of the positions of levels due to the mixing of atomic excitations and surface plasmons, as expected according to Fig. 1. The structure due to the size quantization does not appear in this case either.

The electron energy loss spectrum for the scattering forward for Kr precipitates in Fig. 4 shows quite a significant shift of the position of the atomic excitations expected at 10.19 eV for the bulk Kr. The peak of the surface plasmons is significantly shifted as well. In between these two major peaks, there is a weak structure that corresponds to the excitations of the quantized states in the precipitate. The two large peaks that appear in Fig. 4 are due to the mixed states of the excitons inside the precipitates and the localized plasmons. The energy of the bottom of the exciton band is below the frequency of the localized plasmons, thus the lowest of

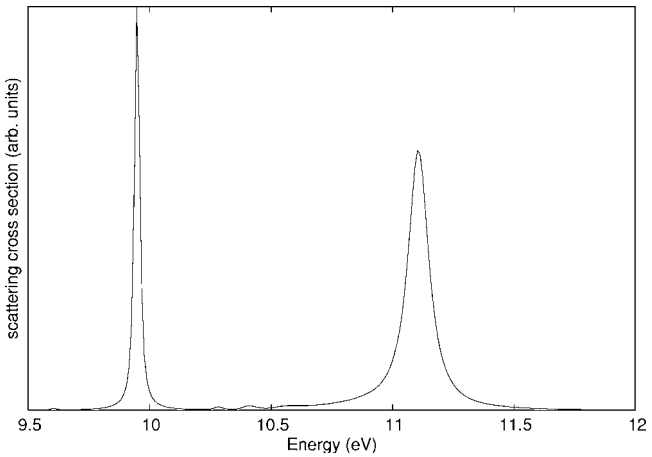

FIG. 3. EELS spectrum for Al with Kr precipitates for the scattering forward. Parameters of the Kr crystal in the precipitates are ω_0=10.19 eV, ω_{LT}=0.12 eV, ε_0=1.88, $M=2.2m_0$.

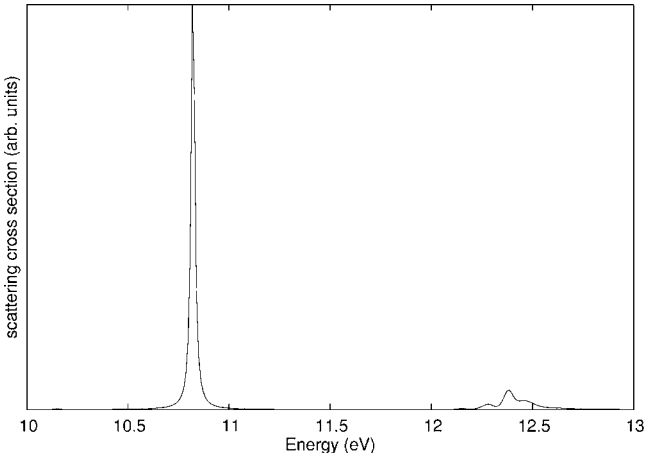

FIG. 4. EELS spectrum for Al with Ar precipitates for the scattering forward. Parameters of the Ar crystal in the precipitates are ω_0=12.06 eV, ω_{LT}=0.15 eV, ε_0=1.66, $M=2.22m_0$.

the peaks should be attributed mainly to the polaritonic state shifted to the low-energy side of the bottom of the exciton band due to interaction with the free electron gas of the host metal. The weak structure between the two major peaks is due to the proper exciton states.

The quantization is more pronounced in the electron energy loss spectrum for $\Theta=0$ for Ar precipitates in Al, as seen in Fig. 5. The main peak of the atomic excitations is strongly shifted from the bottom of the exciton band at 12.06 eV. It is surrounded by a distinct structure due to the size quantization effect.

A similar structure is seen in the spectrum for Ne and He precipitates shown in Figs. 5 and 6, respectively. In these cases, the interaction with surface plasmons is not significant as the bottoms of the exciton bands for those rare-gas crystals are above the plasmon frequency for the metal.

Among the levels of the discrete spectrum, those that are closest to the level of the surface polariton manifest themselves most strongly as one can see in Figs. 4–6.

The contribution of the higher harmonics may be seen in the electron energy loss spectra for nonzero scattering

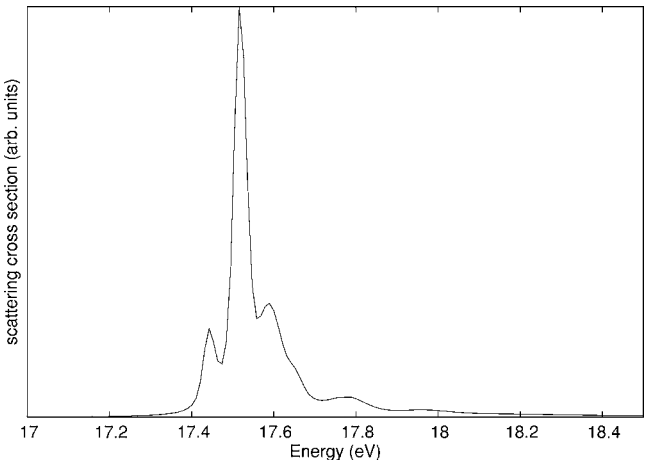

FIG. 5. EELS spectrum for Al with Ne precipitates for the scattering forward. Parameters of the Ne crystal in the precipitates are ω_0=17.36 eV, ω_{LT}=0.2 eV, ε_0=1.24, $M=2.22m_0$.

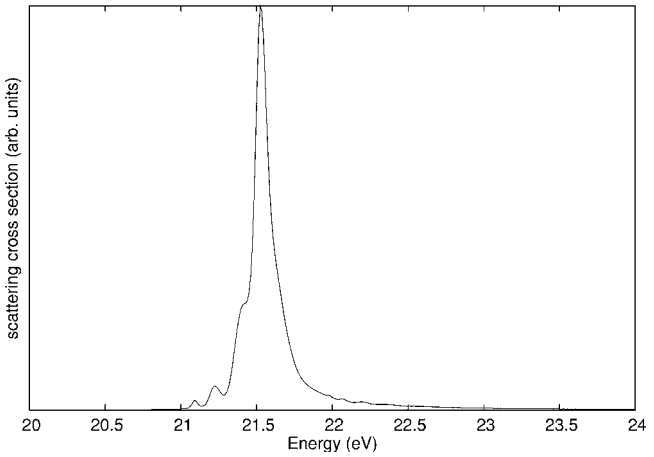

FIG. 6. EELS spectrum for Al with He precipitates for the scattering forward. Parameters of the He crystal in the precipitates are $\omega_0=21.0$ eV, $\omega_{LT}=1.0$ eV, $\varepsilon_0=1.0$, $M=2.2m_0$.

angles. The scattering forward spectra contain mainly the dipole excitations with $l=1$. In the case of $\Theta \neq 0$, the levels for which l is of the order of QR would be the strongest. It is necessary to note, however, that the intensity of the scattering strongly drops with increasing the angle.

The evolution of the shape of the spectrum with increasing the scattering angle is shown in Fig. 7 for Ar precipitates. The series of the peaks that appear above 9.0 eV correspond to the localized plasmons with different l. Note that the energies of the surface plasmons with different l depend on the radii of the precipitates insignificantly. As a result the peaks in the EEL spectra are not smeared by the averaging and are quite significantly separated due to the large value of the plasmon frequency in Al. With increasing the scattering angle the strongest peaks with $l=1$ gradually disappear and become comparable with the peaks with $l=2$, which is noticeable in the next curve. The third curve shows the situation where several different l contribute comparably to the EELS spectrum. The series of peaks converges to the frequency of surface plasmons on a flat surface. This trend is visible in the case of the highest curve.

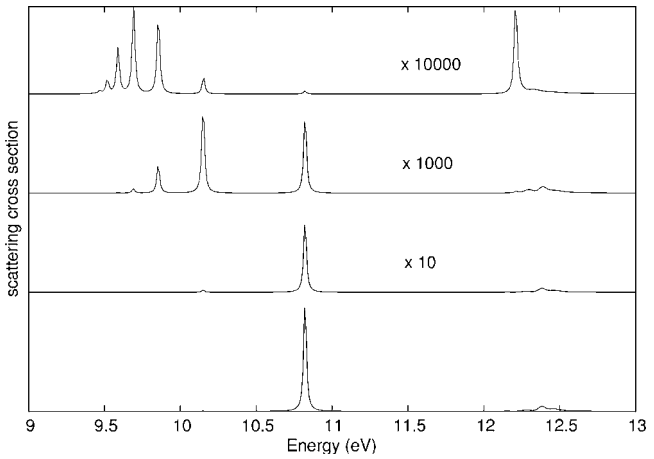

FIG. 7. EELS spectrum for Al with Ar precipitates for different scattering angles $\Theta=0.0$ (the lowest curve), 0.001, 0.005, 0.01.

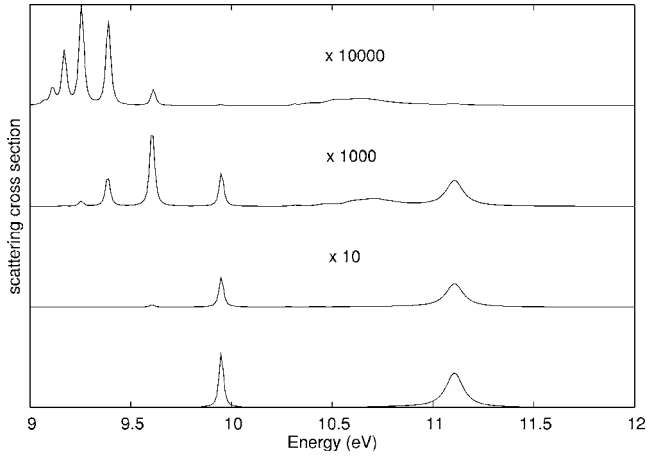

FIG. 8. EELS spectrum for Al with Kr precipitates for different scattering angles $\Theta=0.0$ (the lowest curve), 0.001, 0.005, 0.01.

A similar evolution of the spectrum with increasing the scattering angle is shown in Fig. 8 for the case of Kr precipitates in Al. The interpretation of the spectrum is more difficult in this case. The bottom of the exciton band for Kr is at 10.19 eV, which is very close to the frequency of the surface plasmon with $l=1$ at approximately 10.5 eV. Therefore, for $l=1$ the lowest of the peaks is rather the polaritonic excitation than the localized plasmon, as the energy of the localized plasmon is shifted toward the blue side of the spectrum. At the same time the frequencies of the localized plasmons with $l>1$ are situated below the bottom of the exciton band and experience a red shift due to the mixing with the excitonic states in the Kr precipitates. The excitonic states with $l>1$ move to the higher energies due to the mixing with plasmons, but the value of the shift is not the same as the shift of the energy of the localized plasmon with $l>1$. Figure 8 shows that for the larger values of the scattering angles a broad plateau at a new place appears above the frequency of the bottom of the exciton band. The excitonic levels undergo size-dependent quantization and, therefore, their positions depend on the radii of the precipitates. Due to this reason the contribution of the quantized states is spread over a significant region, forming a plateau.

V. CONCLUSIONS

The electron energy loss spectra of the nanosize rare-gas precipitates in the metal matrix has been considered, taking into account effects of size quantization of the excitations inside the precipitates and their interaction with the free electron gas in the host metal. The manifestation of the excitonic levels and their quantization is most pronounced for the cases where the mixing of two different types of excitations, excitons and localized plasmons, is strongest. In the row of the noble gases, this is realized for Kr and Ar precipitates. For the small angle scattering the structure of the electron energy loss spectra is caused by the quantization of the exciton levels while the magnitude of the scattering is enhanced by the interaction with the localized plasmons. The spectra of the electron losses for greater angles provide the

possibility of observing higher harmonics of the excitations, which is impossible in the optical spectra. The energy difference of the levels corresponding to the excitations with different l can be large (more than 0.5 eV). The experimental study of the EELS for the rare-gas precipitates may be useful for the determination of the parameters of the precipitates such as size of the precipitates, effective mass of the excitons in high-density noble gas crystals, etc.

[1] V. N. Chernikov, W. Kosternich, and H. Ullmaire, J. Nucl. Mater. **227**, 157 (1996).

[2] J. H. Evans and D. J. Mazey, J. Phys. F: Met. Phys. **15**, L1 (1985).

[3] S. E. Donnely, J. C. Rife, J. M. Gilles, and A. A. Lucas, J. Nucl. Mater. **93/94**, 767 (1980).

[4] W. Jager, R. Manzke, H. Trinkaus, G. Crecelius, R. Zeller, J. Fink, and H. L. Bay, J. Nucl. Mater. **111/112**, 674 (1982).

[5] S. E. Donnelly, A. A. Lucas, and J. P. Vigneron, Radiat. Eff. **78**, 337 (1983).

[6] D. I. Potter and C. J. Rossouw, J. Nucl. Mater. **161**, 124 (1989).

[7] H. Pattyn, P. Hendrickx, J. Odeurs, and S. Buckhpan, Mater. Sci. Eng., A **115**, 103 (1989).

[8] D. R. G. Mitchell, S. E. Donelly, and J. H. Evans, Philos. Mag. A **61**, 531 (1990).

[9] P. B. Johnson and D. J. Mazey, J. Nucl. Mater. **218**, 273 (1995).

[10] F. E. Lawson and P. B. Johnson, J. Nucl. Mater. **252**, 34 (1998).

[11] K. Mitsuishi, M. Kawasaki, M. Takeguchi, and K. Furuya, Phys. Rev. Lett. **82**, 3082 (1999).

[12] M. Harting, M. Yaman, R. Bucher, and D. T. Britton, Adv. Eng. Mater. **4**, 592 (2002).

[13] K. Mitsuishi, M. Song, K. Furuya, C. W. Allen, R. C. Birtcher, and U. Dahmen, Nucl. Instrum. Methods Phys. Res. B **206**, 109 (2003).

[14] J. S. Pedersen, A. Horsewell, and M. Eldrup, J. Phys.: Condens. Matter **8**, 8431 (1996).

[15] M. J. W. Greuter and L. Nielsen, J. Phys.: Condens. Matter **5**, 3541 (1993).

[16] I. Yu. Goliney and V. I. Sugakov, Fiz. Nizk. Temp. **11**, 775 (1985).

[17] I. Yu. Goliney and V. I. Sugakov, Phys. Rev. B **62**, 11177 (2000).

[18] I. Yu. Goliney and V. I. Sugakov, Ukr. Fiz. Zh. (Russ. Ed.) **33**, 222 (1988).

[19] A. von Felde and J. Fink, Phys. Rev. B **31**, 6917 (1985).

[20] S. I. Pekar, Zh. Eksp. Teor. Fiz. **34**, 2964 (1958).

[21] *Kryokrystaly*, edited by B. I. Verkiv and A. F. Prikhotko (Naukova Dumka, Kiev, 1983), p. 528 (in Russian).